

REPORT

Deubiquitinating enzyme USP30 maintains basal peroxisome abundance by regulating pexophagy

Victoria Riccio^{1,2} , Nicholas Demers^{1,2}, Rong Hua², Miluska Vissa², Derrick T. Cheng^{1,2}, Amy Wong Strilchuk^{1,2}, Yuqing Wang^{1,2}, G. Angus McQuibban¹, and Peter Kijun Kim^{1,2} 

The regulation of organelle abundance is critical for cell function and survival; however, the mechanisms responsible are not fully understood. In this study, we characterize a role of the deubiquitinating enzyme USP30 in peroxisome maintenance. Peroxisomes are highly dynamic, changing in abundance in response to metabolic stress. In our recent study identifying the role of USP30 in mitophagy, we observed USP30 to be localized to punctate structures resembling peroxisomes. We report here that USP30, best known as a mitophagy regulator, is also necessary for regulating pexophagy, the selective autophagic degradation of peroxisomes. We find that overexpressing USP30 prevents pexophagy during amino acid starvation, and its depletion results in pexophagy induction under basal conditions. We demonstrate that USP30 prevents pexophagy by counteracting the action of the peroxisomal E3 ubiquitin ligase PEX2. Finally, we show that USP30 can rescue the peroxisome loss observed in some disease-causing peroxisome mutations, pointing to a potential therapeutic target.

Introduction

Peroxisomes are vital metabolic organelles present in virtually all eukaryotic cells. In humans, their main function is to break down very long chain and branched fatty acids and oxidize hydrogen peroxide (Smith and Aitchison, 2013). They are also involved in specialized lipid synthesis including bile acids, plasmalogens, and farnesyl-diphosphate, a key cholesterol precursor (Wanders and Waterham, 2006). While deficiencies in peroxisomes are linked to many neurological disorders including Alzheimer’s disease and amyotrophic lateral sclerosis, our understanding of peroxisomes’ roles in disease etiology is in its infancy (Trompier et al., 2014). The best-characterized peroxisomal diseases are peroxisome biogenesis disorders (PBDs), a group of autosomal recessive developmental disorders caused by the absence of peroxisomes (Braverman et al., 2016).

Selective autophagy is a key process to maintaining organelle abundance and health within the cell. It is a conserved cellular process by which specific organelles or other large cytoplasmic materials are targeted and sequestered by autophagosomes, a double membrane compartment that fuses with lysosomes to degrade its contents (Klionsky et al., 2016). In mammalian cells, protein ubiquitination signals organelles for degradation (Klionsky et al., 2016). Two organelles that undergo selective autophagy are mitochondria and peroxisomes, termed mitophagy and pexophagy, respectively. During mitophagy, ubiquitin is added by the E3 ligase Parkin that translocates from the cytosol

to the outer membrane of damaged mitochondria, resulting in increased ubiquitination and autophagosome sequestration (Youle and Narendra, 2011). Parkin ubiquitination is antagonized by several deubiquitinating enzymes, including USP30 and USP35, both localized to the outer mitochondrial membrane (Wang et al., 2015).

Pexophagy is induced by various cellular stresses including starvation and hypoxia (Nordgren et al., 2013). During amino acid starvation, the levels of the peroxisomal E3 ubiquitin ligase PEX2 rise, resulting in increased peroxisome membrane protein ubiquitination, followed by the recruitment of the autophagy receptors NBR1 and p62 and autophagosome sequestration (Deosaran et al., 2013; Sargent et al., 2016). However, it is not known whether a peroxisomal-specific deubiquitinating enzyme regulates pexophagy.

In our previous study characterizing the role of USP30 in mitophagy, we observed USP30 localized to small punctate structures that resembled peroxisomes (Wang et al., 2015). Interestingly, USP30 artificially targeted to peroxisomes was shown to reduce pexophagy (Cunningham et al., 2015). Therefore, we hypothesized that if peroxisomes are a bona fide location for USP30, then it may have a role in regulating pexophagy. In this study, we characterized the subcellular localization of USP30 and systematically demonstrate USP30 to be a regulator of pexophagy.

¹Biochemistry Department, University of Toronto, Canada; ²Cell Biology Department, Hospital for Sick Children, Toronto, Canada.

Correspondence to Peter Kijun Kim: pkim@sickkids.ca; G. Angus McQuibban: angus.mcquibban@utoronto.ca.

© 2019 Riccio et al. This article is distributed under the terms of an Attribution–Noncommercial–Share Alike–No Mirror Sites license for the first six months after the publication date (see <http://www.rupress.org/terms/>). After six months it is available under a Creative Commons License (Attribution–Noncommercial–Share Alike 4.0 International license, as described at <https://creativecommons.org/licenses/by-nc-sa/4.0/>).

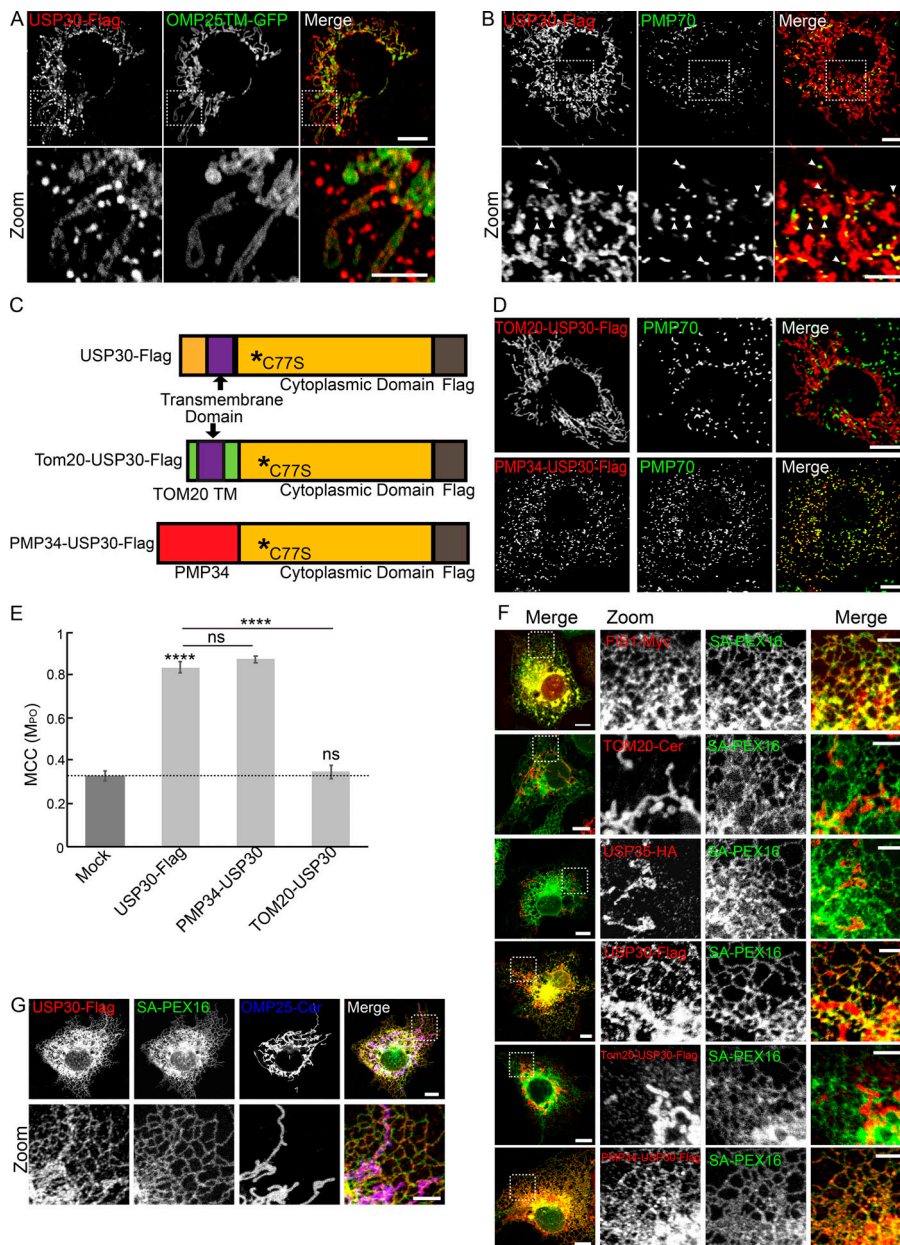


Figure 1. Overexpressed USP30 localizes to peroxisomes. (A and B) COS7 cells expressing USP30-Flag (red) and mitochondrial marker OMP-25-GFP (A) or stained for peroxisome marker PMP70 (green; B). **(C)** Schematic of USP30-Flag, PMP34-USP30-Flag, and TOM20-USP30-Flag constructs show the site of the catalytic mutation (*C77S). **(D)** COS7 cells expressing TOM20-USP30-Flag or PMP34-USP30-Flag (red) and stained for PMP70 (green). **(E)** Thresholded MCC of PMP70-stained peroxisomes (M_{po}) colocalized with USP30-Flag, PMP34-USP30, TOM20-USP30, or ATP5A (mock). **(F)** COS7 cells expressing SA-PEX16-GFP (green) with mitochondrial proteins FIS1-Myc, TOM20-Cer, USP35-HA, or USP30 constructs (red) as indicated. Mitochondrial localization shown in Fig. S1 G. **(G)** COS7 coexpressing USP30-Flag (red), sa-PEX16 (green), and OMP25-Cer (blue). Statistical significance (Student's *t* test): ****, $P \leq 0.0001$; ns, $P \geq 0.05$ ($n = 3$; 30 cells/trial). White boxes indicate zoomed region. Bars: 10 μm ; 5 μm in zoom.

Results and discussion

USP30 localizes to peroxisomes

To determine whether USP30 localizes to peroxisomes, we first examined its subcellular localization in COS7 cells by immunofluorescence microscopy. As expected, USP30-Flag colocalized with the mitochondrial marker OMP25TM-GFP, but was also found in punctate structures that did not contain OMP25TM (Fig. 1 A). These USP30-Flag puncta instead colocalized with the endogenous peroxisomal protein peroxisome membrane protein 70 (PMP70; Fig. 1 B). Similar localization was observed in HeLa cells (Fig. S1 A). Furthermore, subcellular fractionation of USP30-Flag-expressing HeLa cells showed USP30 in the peroxisomal fraction (Fig. S1 B).

Many proteins localize and act on both peroxisomes and mitochondria, including the fission proteins FIS1 and DRP1 (Koch et al., 2005) and the antiviral protein MAVS (Dixit et al.,

2010). However, to confirm that the peroxisomal localization of USP30-Flag was not an artifact of overexpression, we constructed TOM20-USP30-Flag, a USP30 construct in which its N-terminal transmembrane domain was replaced by the N-terminal transmembrane domain of the mitochondria membrane protein TOM20 (Fig. 1 C). We argue that if the peroxisome localization of USP30 is a mis-targeting artifact of overexpressing a mitochondrial membrane protein, then TOM20-USP30 should also mis-target upon overexpression. As a peroxisome-targeting control, USP30 was fused to the C terminus of the peroxisomal membrane protein PMP34 (PMP34-USP30-Flag; Fig. 1 C). We found that TOM20-USP30 did not localize to peroxisomes, as seen in the immunofluorescence (Fig. 1 D and Fig S1 C) and cell fractionation (Fig. S1 D). In contrast, PMP34-USP30 localized exclusively to peroxisomes (Fig. 1 D and Fig S1, E and F). Further, colocalization between

peroxisomes and USP30 was quantified in HeLa cells demonstrating this localization (Fig. 1 E).

Next, we examined whether the peroxisomal import machinery can target USP30 to peroxisome membranes. PEX16 recruits most, if not all, membrane proteins to the peroxisome through the ER, as the ER localized sa-PEX16, a PEX16 construct with an ER-targeting stop-anchor sequence (sa-PEX16) can import PMPs to the ER (Hua et al., 2015). Here, we found that sa-PEX16 recruited the dual mitochondria and peroxisome-targeted FIS1 to the ER, but not the mitochondrial proteins TOM20 and USP35 (Fig. 1 F and Fig. S1, G and H; Wang et al., 2015). When the different USP30 constructs were coexpressed with saPEX16, both the WT USP30 and PMP34-USP30 but not TOM20-USP30 were recruited to the ER (Fig. 1 F), suggesting that USP30 can be targeted by PEX16 in a mechanism similar to other PMPs. Interestingly, USP30-Flag was still found on mitochondria (Fig. 1 G), suggesting that targeting to both organelles is likely independent and competitive.

Overexpression of USP30 prevents peroxisome loss during amino acid starvation

USP30 overexpression has been shown to reduce mitophagy (Bingol et al., 2014), but based on its peroxisomal localization, we next investigated its effects on pexophagy. Pexophagy was induced by amino acid starvation (herein referred as starvation) with HBSS, which causes a reduction in peroxisomes after 24 h (Fig. 2 A; mock). To compare changes in peroxisome numbers, we determined the peroxisome density per cell, which is the total number of PMP70 puncta over the cell volume. Here we observed a significant decrease in peroxisome density in HBSS-treated cells compared with control (DMEM) cells (Fig. 2 B). However, this loss of peroxisomes upon HBSS treatment was prevented by the expression of either USP30-Flag or PMP34-USP30, but not TOM20-USP30 (Fig. 2, A and B). Similar results were also observed by immunoblot analysis for the peroxisomal membrane protein PEX14, where PEX14 loss was not merely inhibited upon the expression of USP30 but increased (Fig. 2, C and D). In addition, TOM20-USP30 did not prevent the loss of PEX14 during starvation (Fig. S2 A).

To determine whether USP30 deubiquitinase activity is required to prevent peroxisome loss during starvation, we tested a catalytic mutant (USP30-Flag C77S), in which cysteine at residue 77 was changed to serine (Nakamura and Hirose, 2008). This mutation has previously been shown to abolish the protective effects of USP30 on mitophagy upon carbonyl cyanide *m*-chlorophenyl hydrazone (CCCP) treatment (Liang et al., 2015). We found that USP30-Flag C77S and PMP34-USP30 C77S were unable to prevent peroxisome loss (Fig. 2, B and E), suggesting that USP30's deubiquitination activity is required to prevent starvation-induced peroxisome loss.

Finally, to test whether USP30 prevents pexophagy, we examined the targeting of peroxisomes to lysosomes using a pH-sensing autophagy assay, the red-green (RG) assay (Deosaran et al., 2013). The RG assay utilizes a peroxisome-targeted construct, consisting of the transmembrane domain of PEX26 tandem-tagged with GFP and RFP (PEX26_{TM}-RG). While both fluorophores are fluorescent in the neutral cytosol, GFP

fluorescence is quenched in the acidic lysosome, resulting in RFP fluorescence only. When PEX26_{TM}-RG was expressed alone, increased red signal was observed under starvation, indicating increased lysosomal targeting of peroxisomes (Fig. 2, F and H). When we coexpressed PEX26_{TM}-RG with USP30-Flag, the increase in the RFP-only signal was not observed during starvation (Fig. 2, G and H), demonstrating that USP30 can prevent starvation-induced pexophagy. Together, these results suggest that peroxisomally localized USP30 prevents starvation-induced pexophagy.

USP30 maintains peroxisome numbers under basal conditions

Next, we asked whether USP30 is required for maintaining peroxisome numbers under basal growth conditions. Here, we performed siRNA-mediated knockdown to deplete cells of endogenous USP30. Using quantitative immunofluorescence microscopy to measure peroxisome abundance (Fig. 3, A and B) and immunoblot analysis for PEX14 (Fig. 3, C and D), we found a reduction in peroxisome levels under basal condition, similar to levels observed during only starvation.

To determine whether the peroxisome loss in USP30-depleted cells was mediated by autophagy, we depleted USP30 in the autophagy-deficient ATG5 knockout mouse embryonic fibroblast (MEF) cells (ATG5^{-/-}). ATG5 is an autophagy protein responsible for phagophore elongation, and its absence inhibits autophagy (Kuma et al., 2004). Compared with WT MEFs, peroxisome loss was not observed in ATG5^{-/-} MEFs when USP30 was depleted (Fig. 3, E and F). Similarly, inhibiting autophagy by treatment with the lysotropic drug chloroquine (Fig. 3, G and H), or by codepletion of the autophagy factor ATG12 (Fig. 3, I and J), also prevented peroxisome loss in USP30-depleted HeLa cells. This further supports that USP30 depletion-induced peroxisome loss is autophagy mediated. Similarly the loss of peroxisomes was also prevented in USP30-deficient cells when codepleted of NBR1 (Fig. 3, I and J), an autophagy receptor that binds ubiquitinated peroxisomes (Deosaran et al., 2013; Yamashita et al., 2014). Collectively, these data suggest USP30 regulates basal pexophagy.

USP30 and PEX2 antagonize each other

During starvation, the abundance of the E3 ligase PEX2 increases in response to mTORC1 inhibition, resulting in peroxisomal membrane protein ubiquitination (Sargent et al., 2016). To test whether PEX2 is required for peroxisome loss in cells depleted of USP30, we codepleted USP30 and PEX2 using siRNAs and found that the peroxisome loss was prevented in both basal and starvation conditions (Fig. 3, K and L). This suggests that PEX2 is required for pexophagy under basal conditions and that USP30 counters the action of PEX2 to maintain basal peroxisome numbers.

USP30 inhibits pexophagy by preventing ubiquitination of peroxisome membrane proteins

PEX5 is a shuttle protein involved in peroxisome matrix protein import. It is ubiquitinated at the peroxisomal membrane as part of its general import cycle, allowing it to be recycled back to the cytosol (Wang and Subramani, 2017). Peroxisomes that lose the

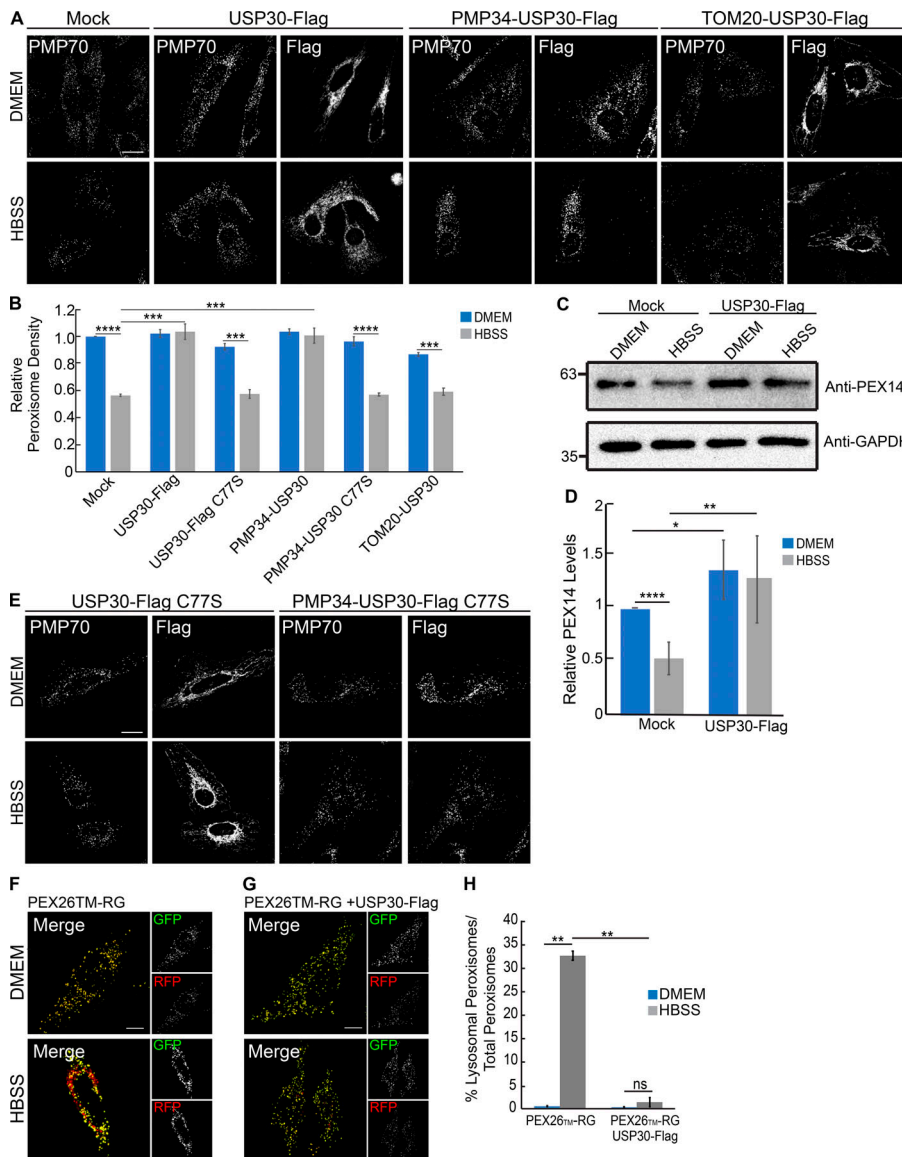


Figure 2. Overexpressed USP30 reduces peroxisome loss induced by starvation. (A) Immunofluorescence of HeLa cells transfected with USP30-Flag, PMP34-USP30-Flag, or TOM20-USP30-Flag or mock transfected. Cells grown in DMEM or HBSS for 24 h, stained for PMP70 and Flag. **(B)** Quantification of the peroxisome density in A and E, relative to mock DMEM ($n = 3$; 30 cells/trial). **(C)** HeLa lysates expressing USP30-Flag, analyzed by immunoblotting for PEX14 and GAPDH. **(D)** Quantification of PEX14/GAPDH density ratio in C compared with mock DMEM ($n = 6$). **(E)** HeLa cells expressing USP30-Flag C77S or PMP34-USP30-Flag C77S, costained for PMP70. **(F and G)** HeLa cells expressing PEX26-RG alone (F) or coexpressed with USP30-Flag (G). **(H)** Quantification of average percent lysosomal peroxisomes ($n = 3$; 50 cells/trial). Statistical significance (Student's *t* test): *, $P \leq 0.05$; **, $P \leq 0.01$; ***, $P \leq 0.001$; ****, $P \leq 0.0001$. Bars: 20 μm (A and E); 10 μm (F and G).

ability to remove ubiquitinated PEX5 from the membrane have been shown to be degraded by pexophagy (Nuttall et al., 2014; Law et al., 2017). Ubiquitinated PEX5 was also shown to mediate pexophagy during oxidative stress (Nordgren et al., 2015; Zhang et al., 2015). These studies suggest that aberrant PEX5 recycling resulting in accumulation of ubiquitinated PEX5 on the membrane may be a major signal for pexophagy. To determine whether ubiquitinated PEX5 is the main signal for starvation-induced pexophagy, we depleted cells of PEX5 followed by starvation. We found that the PEX5 depletion was not sufficient to prevent peroxisome loss during starvation. However, USP30 overexpression was able to rescue starvation-induced peroxisome loss in PEX5-depleted cells (Fig. 4, A and B), suggesting that PEX5 is not the only pexophagy signal during starvation.

Since PEX2 has been shown to ubiquitinate multiple peroxisomal membrane proteins including PEX5 and PMP70 (Sargent et al., 2016), we hypothesized that USP30 is able to deubiquitinate multiple membrane proteins based on ubiquitination status and vicinity, rather than through specific protein recognition.

To test this, we examined the ubiquitination status of these proteins by immunoprecipitating HA-tagged ubiquitin (HA-Ub) from HEK293 cells expressing HA-Ub under a tamoxifen-inducible promoter. Upon USP30 depletion, we observed an increase in ubiquitination of the membrane proteins PEX5 and PMP70, but not the matrix protein catalase (Fig. 4, C and D). This suggests that USP30 counteracts PEX2 by deubiquitinating its substrates.

To further validate that USP30 prevents the accumulation of ubiquitinated proteins on peroxisomes, we examined whether it can prevent the accumulation of the ubiquitin-binding autophagy receptor NBR1 on peroxisomes. We have previously shown that 4-h starvation results in an increase in NBR1 recruitment to peroxisomes (Sargent et al., 2016). We propose that if USP30 prevents pexophagy by removing ubiquitin on peroxisomes, then overexpressing USP30 should prevent NBR1 recruitment to peroxisomes during starvation. Indeed, analysis of colocalization by immunofluorescence microscopy show that overexpressing USP30 prevents the colocalization of NBR1 to peroxisomes

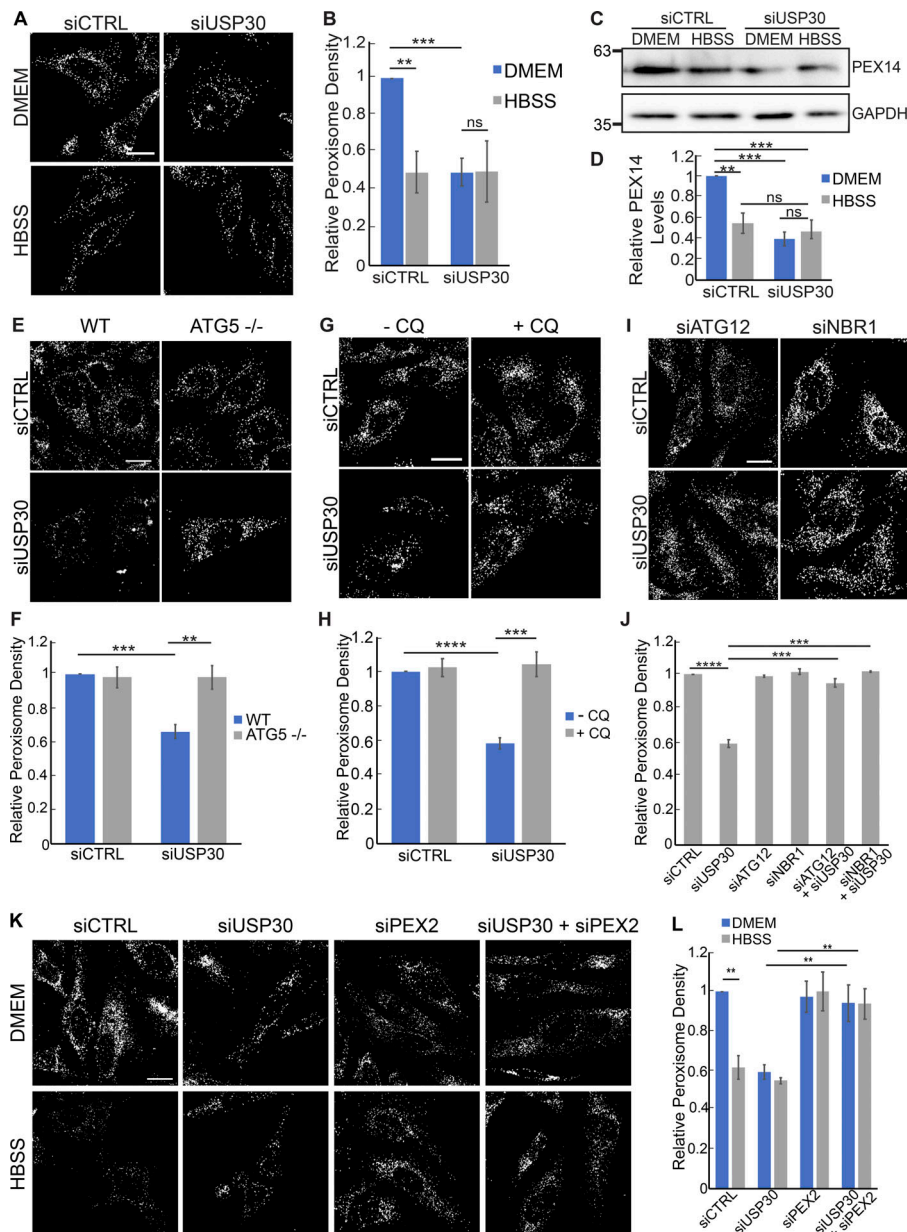


Figure 3. Silencing USP30 induces pexophagy and is opposed by PEX2. (A) Confocal immunofluorescent images of PMP70 in HeLa cells treated with siRNA against USP30 (siUSP30) or a nontargeting siRNA (siCTRL) grown in DMEM or HBSS for 24 h. (B) Quantification of the relative peroxisome density in A, relative to siCTRL DMEM. (C) Immunoblots of PEX14 and GAPDH in HeLa cells treated with siRNA as in A. (D) Average PEX14 levels in C, compared with GAPDH levels and normalized to siCTRL DMEM. (E) ATG5 WT and ATG5^{-/-} MEFs, treated with siCTRL or siUSP30, under DMEM or HBSS, stained for PMP70. (F) Quantification of E, with all treatment values relative to siCTRL ATG5 WT. (G) HeLa cells treated with siCTRL or siUSP30 were incubated with 5 μM of chloroquine (CQ) and stained for PMP70. (H) Quantification of G relative to siCTRL -CQ. (I) HeLa cells treated with siATG12 or siNBR1 cotreated with either siCTRL or siUSP30, stained for PMP70. (J) Quantification of I relative to siCTRL treatment. (K) Cells treated with siRNA against PEX2 (siPEX2) and codepleted of siUSP30 or siCTRL. Cells were grown in either DMEM or HBSS for the final 24 h and stained for PMP70. (L) Quantification of K, with all treatment groups relative to DMEM siCTRL. Statistical significance (Student's *t* test): **, *P* ≤ 0.01; ***, *P* ≤ 0.001; ****, *P* ≤ 0.0001; ns, *P* ≥ 0.05; *n* = 3; 50 cells/trial. Bars, 20 μm.

during starvation (Fig. 4, E and F). This further supports the hypothesis that USP30 prevents pexophagy by removing ubiquitin on peroxisomes.

USP30 overexpression rescues peroxisome loss in PEX1- and PEX26-deficient cells

PBDs are rare genetic diseases resulting from a lack of functional peroxisomes. The most common mutations occur in PEX1, a component of the peroxisomal ATPases associated with diverse cellular activities (AAA ATPase), which is composed of PEX1, PEX6, and PEX26 (Braverman et al., 2016). Defects in this gene were originally thought to reduce peroxisome numbers by inhibiting peroxisome formation. However, our work suggests that the loss in AAA ATPase activity results in an accumulation of ubiquitinated PEX5, signaling pexophagy (Law et al., 2017). This suggests that an alternative method of removing ubiquitinated PEX5 from peroxisomes in

AAA ATPase defective cells may prevent peroxisome loss. To test this hypothesis, we investigated whether overexpressing USP30 can complement cells with defective AAA ATPase function. As previously shown, knockdown of PEX1 or PEX26 resulted in a loss of peroxisomes, but was rescued by USP30-Flag and PMP34-USP30 overexpression (Fig. 5, A and B; and Fig S3, A-C).

Next, we examined whether USP30 can rescue peroxisome deficiency in a PBD fibroblast cell line with the most common PEX1 mutation, PEX1 G843D. Compared with control fibroblast cells, PEX1 G843D cells have significantly fewer peroxisomes (Fig. 5, C and D). Strikingly, overexpressing USP30-Flag and PMP34-USP30, but not catalytically inactive USP30-C77S, increased the number of peroxisomes in the PEX1 G843D fibroblasts (Fig. 5, C and D; and Fig. S3, D and E). Collectively, these data suggest that USP30 can rescue peroxisome loss induced by AAA ATPase deficiency.

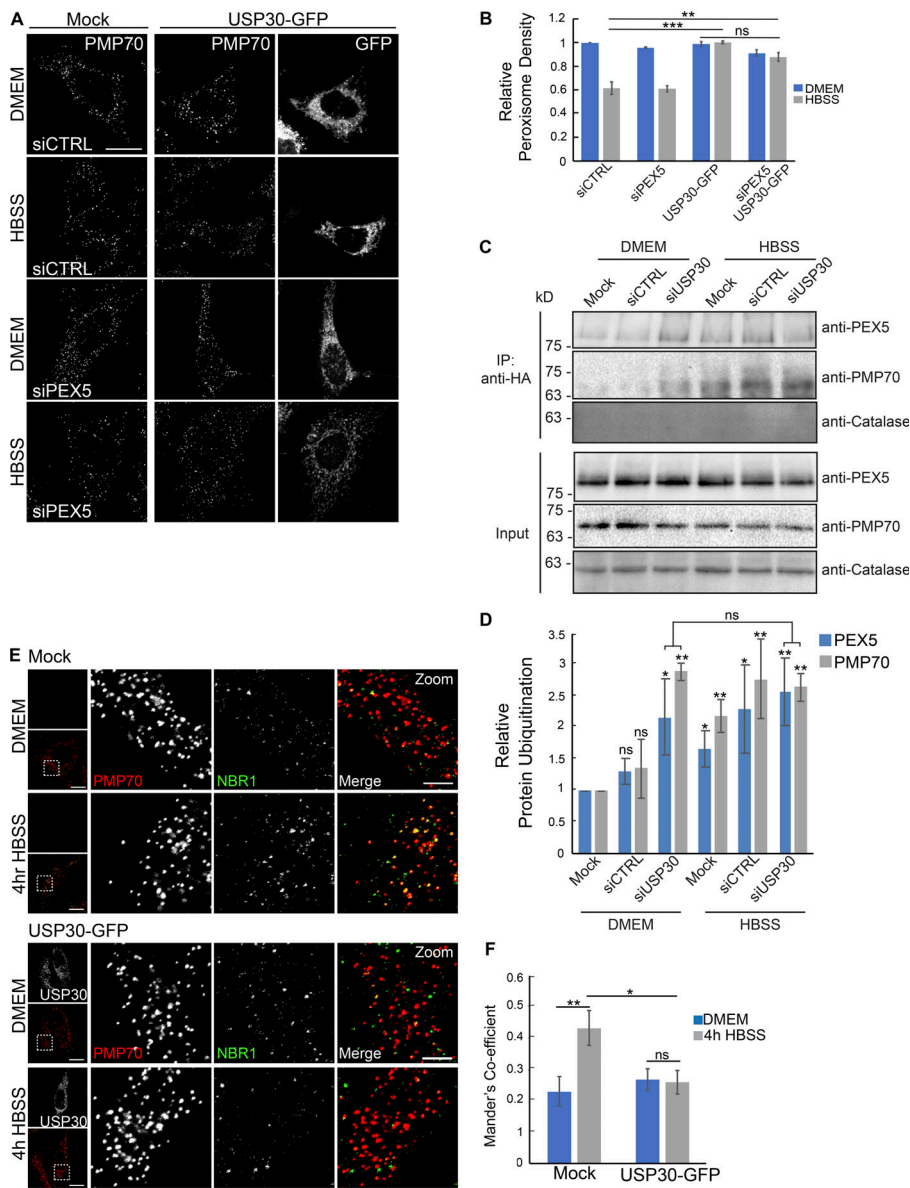


Figure 4. Knockdown of USP30 results in increased ubiquitinated PEX5 and PMP70. (A) Knockdown of PEX5 (siPEX5) in HeLa cells, with overexpression of USP30-GFP grown in DMEM or HBSS for 24 h. Cells stained for PMP70. (B) Quantification of A, all treatment values relative to siCTRL DMEM. (C) Immunoprecipitation of HA-Ub, performed in HEK293 cells stably expressing HA-Ub. Cells were mock-treated or treated with siCTRL or siUSP30 under DMEM and HBSS conditions, probing for PMP70, PEX5, and catalase. (D) Quantification of PEX5 and PMP70 levels immunoprecipitated in C, relative to mock-treated DMEM. Each condition was normalized to the input. (E) HeLa cells stained for endogenous NBR1 (green) and PMP70 (red), either mock transfected or overexpressing USP30-GFP (white). (F) MCC of PMP70 (or M_{po}) colocalized with NBR1 representative images in E. Statistical significance (Student's *t* test): *, $P \leq 0.05$; **, $P \leq 0.01$; ***, $P \leq 0.001$; ns, $P \geq 0.05$; $n = 3$; 30 cells/trial. Bars: 20 μ m and 5 μ m in zoom.

We were unable to fully assess endogenous USP30 localization; however, a report by Marcassa et al. (2018) published during the preparation of this manuscript demonstrated that endogenous USP30 localizes to peroxisomes and regulates basal pexophagy. Based on our findings, we propose a model whereby the opposing action of the E3 ubiquitin ligase PEX2 and the deubiquitinating enzyme USP30 maintains peroxisome numbers (Fig. 5, E and F). We further propose that peroxisome levels can be regulated by modulating their expression, where an increase in USP30 will result in an increase in peroxisome numbers, while an increase in PEX2 reduces peroxisome numbers. Our work also suggests that the regulation of both peroxisomes and mitochondria may be more interconnected than previously thought. It has been known that the two organelles share the same components for their proliferation (Schrader et al., 2016). Here, we show that a mitophagy regulator, USP30, also regulates pexophagy. However, it has yet to be determined why the two organelles share a common regulator, especially given that

mitophagy and pexophagy are differentially regulated during starvation (Rambold et al., 2011). Finally, our finding that USP30 may complement cells deficient in PEX1 function suggests the potential therapeutic utility of USP30. We found that overexpressing USP30 was sufficient to double the peroxisome numbers in PEX1-deficient cells, suggesting that any mechanism that increases USP30 expression and/or activity may help circumvent peroxisome loss in PEX1-deficient cells. Therefore, future work on regulation of USP30 may provide new targets and tools for studying pexophagy in human health and disease.

Materials and methods

Plasmids and primers

The following plasmids were previously described: USP30-GFP, OMP25TM-GFP, OMP25TM-Cer, sa-PEX16-GFP, Fis1-Myc, PEX26_{TM}-RG, USP35-HA, and TOM20-Cer (Deosaran et al., 2013; Hua et al., 2015; Wang et al., 2015). The following plasmids were

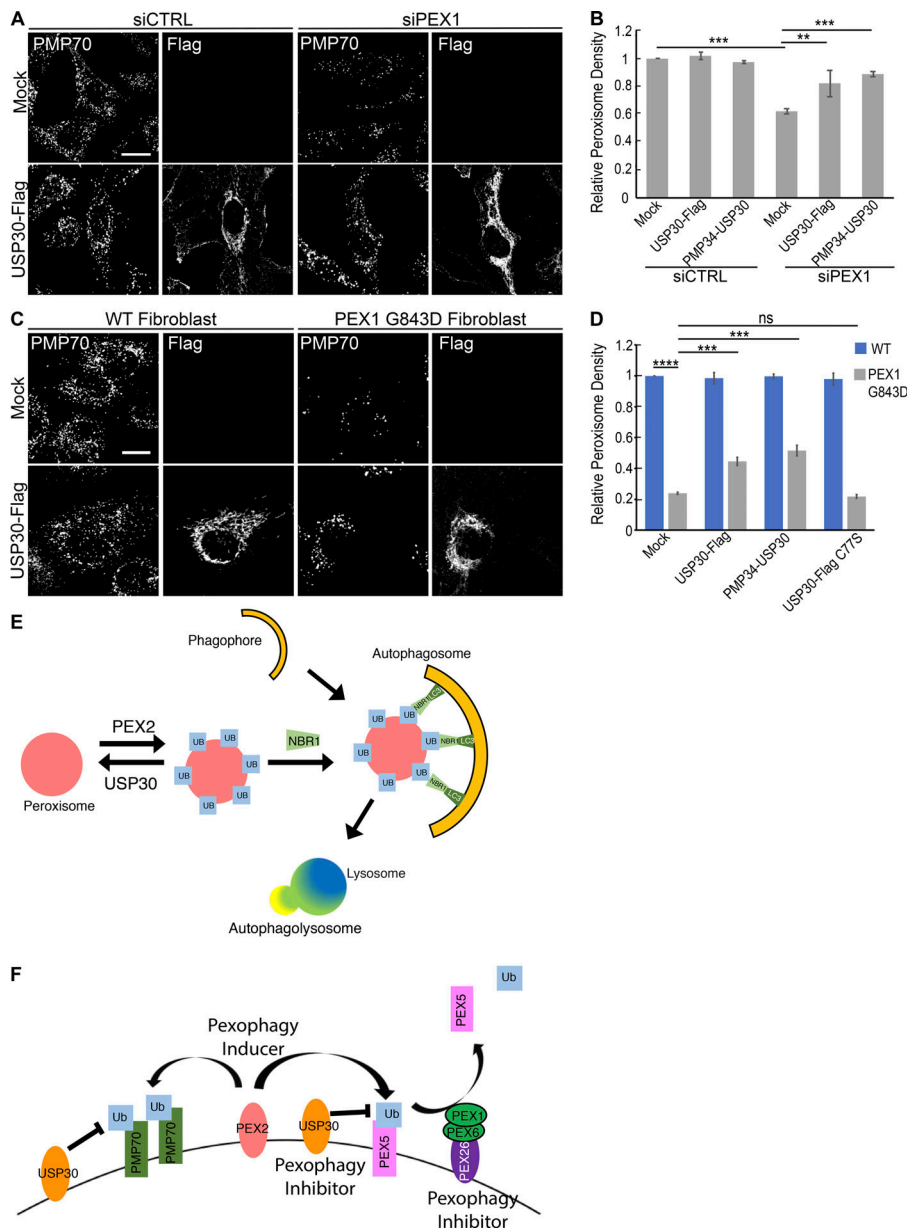


Figure 5. USP30 overexpression can rescue peroxisome levels induced by mutation of the AAA ATPase. (A) HeLa cells treated with siRNA against PEX1 (siPEX1) or siCTRL, then mock-transfected or transfected with USP30-Flag, costained for PMP70. (B) Quantification of A with all treatment values calculated relative to mock siCTRL. Representative images for PMP34-USP30 are found in Fig. S2 A. (C) Human fibroblast cells from healthy (WT) or PEX1 G843D mutation overexpressing USP30-Flag and imaged as in A. (D) Quantification of peroxisome density with respect to mock-treated WT cells in C. (E) Model of PEX2 and USP30 in pexophagy. Peroxisomes are maintained by a balance between the action of USP30 and PEX2. Excess of PEX2 results in pexophagy. (F) PEX2 is responsible for ubiquitinating PMP70 and PEX5. PMP70 is deubiquitinated by USP30, while PEX5 can be removed by the AAA ATPase or deubiquitinated by USP30. Statistical significance (Student's *t* test): **, $P \leq 0.01$; ***, $P \leq 0.001$; ****, $P \leq 0.0001$; ns, $P \geq 0.05$; $n = 3$; 30 cells/trial. Bars, 20 μm .

constructed for this study: USP30-Flag, PMP34-USP30-Flag, TOM20-USP30-Flag, USP30-Flag C77S, and PMP34-USP30-Flag C77S. The USP30 open-reading frame used in all the constructs described below was obtained from the USP30-HA and USP30-EGFP plasmids described previously (Wang et al., 2015). USP30-Flag was designed by subcloning USP30 from USP30-EGFP into Flag-N1 (Clontech pEGFP-N1 vector with the EGFP replaced by three tandem Flag tags). TOM20-USP30-Flag was constructed by first PCR-amplifying USP30-Flag (including the stop codon; primers: 5'-ATCGACCGGTCATGCTGAGCTCCGGGC-3' and 5'-ATCGACCGGTTTACTTGTGCATCGTCATCC-3'), then inserting it in between TOM20 and EGFP of TOM20-EGFP (Clontech pEGFP-N1 vector containing the TM domain of TOM20 upstream of the EGFP), and finally using PCR-mediated deletion to remove the transmembrane domain of the USP30 (codons 34–56 of USP30; primers: 5'-GGTAAGCTTACAGAAAGAAAG-3' and 5'-CCAAAGCTTCATGACTTTATATC-3'). PMP34-USP30-Flag was

constructed by PCR-amplifying USP30-Flag (including the stop codon) and then inserting it in between the PMP34 and EGFP of PMP34-EGFP. USP30-Flag C77S and PMP34-USP30-Flag C77S were constructed via site directed mutagenesis of USP30-Flag and PMP34-USP30-Flag, respectively, all changing C77 of USP30 to S (primers: 5'-TTAGGGAACACCTCCTTCATGAAGTCC-3' and 5'-GGAGTTCATGAAGGAGTCCCTAA-3'). The protein expression of these constructs are shown in Fig. S2 B.

Antibodies

The following antibodies were used in this study: rabbit anti-PMP70 (Abcam; ab3421), mouse anti-Flag (Sigma-Aldrich; F3165), rabbit anti-PEX5 (gift from G. Dodt at the University of Tübingen, Tübingen, Germany), mouse anti-HA (BioLegend; MMS-101R), rabbit anti-PEX14 (Millipore; ABC142), rabbit anti-catalase (Millipore Sigma; 219010), mouse anti-NBR1 (Abnova; H00004077-MO1), mouse anti-ATP5A (abcam; ab14748), mouse

anti-Myc (Clontech; 631206), rabbit anti-VAPB (Sigma-Aldrich; HPA013144), goat anti-rabbit IgG-HRP (Thermo Scientific; 31460), anti-GAPDH HRP (Novus Biologicals; NB300-328H), goat anti-mouse IgG-HRP (Cedarlane; CLCC30007), goat anti-mouse IgG Alexa Fluor 488 (Thermo Fisher Scientific; A-11001), goat anti-rabbit IgG Alexa Fluor 568 (Thermo Fisher Scientific; A-11011), and donkey anti-mouse IgG Alexa Fluor 647 (Thermo Fisher Scientific; A-31571).

siRNAs

The following previously validated siRNAs were used, custom synthesized from Sigma-Aldrich: USP30 (5'-CUAGUCAACACA ACCCUAAACU-3'; Wang et al., 2015), PEX26 (5'-CAAGACCCA GCCAAUCAA-3'; Law et al., 2017), PEX1 (5'-CCAAGCAACUUC AGUCAAA-3'; Law et al., 2017), ATG12 (5'-GUGGGCAGUAGA GCGAACA-3'; Deosaran et al., 2013), NBRI (5'-GGAGUGGAU UUACCAGUUUU-3'; Deosaran et al., 2013), PEX5 (5'-GGCAGA GAAUGAACAAAGAACUAUUUA-3'; Law et al., 2017), PEX2 (5'-GCU AGUUUGGUCCCAGUUU-3'; Sargent et al., 2016), and non-targeting control siRNA (5'-AAUAAGGCUAUGAAGAGAUAC-3'). siRNAs were validated using the TaqMan real-time quantitative PCR (RT qPCR) system (Applied Biosystems) or Western blotting (Fig. S2, C-E). For qPCR analysis, total cellular RNAs were isolated using the SV Total RNA Isolation System (Promega), and cDNAs were subsequently synthesized using the High Capacity cDNA Reverse Transcription kit (Applied Biosystems). TaqMan primers were purchased from Thermo Fisher Scientific. qPCR was performed on a StepOne Real Time PCR System using TaqMan Fast Advanced Master Mix, with GAPDH acting as a reference gene for all quantifications.

Cell culture

HeLa, COS7, ATG5 WT, and ATG5 knockout (ATG5^{-/-}) MEFs (Sargent et al., 2016), HA-Ub HEK293 cells (Sargent et al., 2016), and the human WT and PEX1 G843D fibroblast cells (Law et al., 2017) were grown in DMEM (Gibco), supplemented with 10% FBS (Wisent). Cells were cultured at 37°C in humidified air containing 5% CO₂. Plasmids and siRNAs were transfected using Lipofectamine-2000 (Invitrogen) according to the manufacturer's instructions. Plasmids were transfected and allowed to express for 16–24 h before any treatments were applied. Depletion experiments were performed using an siRNA 2-d knockdown protocol, either followed by treatment or plasmid overexpression. For amino acid starvation experiments, cells were subjected to HBSS (Lonza) treatment for 24 h. Chloroquine (chloroquine diphosphate salt; Sigma-Aldrich)-treated cells were subjected to a 2-d knockdown protocol, followed by 24-h HBSS treatment and concurrent treatment with the chloroquine or solvent control.

Microscopy

Confocal fluorescence imaging was performed using a Zeiss LSM710 laser-scanning confocal microscope with a 40× 1.3 NA or 63× 1.4 NA Oil Plan-APOCRAMAT objective and the appropriate lasers and filter. For immunofluorescence, cells were fixed using 3.7% paraformaldehyde (Electron Microscopy Sciences) and subsequently permeabilized with 0.1% Triton X-100 in PBS.

Cells were incubated in the blocking buffer (10% FBS in PBS) for 30 min, followed by incubation with specific antibodies as indicated. Coverslips were then mounted on glass slides using DAKO mounting medium and stored at 4°C. Live cells were imaged at 37°C in humidified air containing 5% CO₂ stage. Brightness and contrast was modified using Adobe Photoshop CS6 (Version 13.0 x64) for the purpose of presentation.

Coimmunoprecipitation and Western blotting

HEK293 cells stably expressing HA-Ub under the control of a tamoxifen promoter were grown in 10-cm dishes and treated as described in the main body. Additionally, 24 h before lysis, cells were treated with 10 μM tamoxifen and 10 μM chloroquine; 3 h before lysis, cells were treated with 10 μM MG132. Cells were lysed in 1 ml of lysis buffer (50 mM Hepes, pH 7.5, 150 mM NaCl, 1% Triton X-100, 10% glycerol, 1.5 mM MgCl₂, and 1.0 mM EGTA), supplemented with protease inhibitor cocktail (BioShop). 1 mg of lysate was incubated with 20 μl of protein G agarose beads (BioShop) and 1 μg of anti-HA antibody overnight at 4°C. Samples were then washed three times with lysis buffer, and protein was eluted by boiling in SDS-containing sample buffer for 5 min. Samples were then analyzed by standard immunoblot procedures. For other Western blotting analysis, cell were lysed using lysis buffer containing 100 mM Tris-HCl, 1% SDS, and protease inhibitor cocktail (BioShop). Proteins were visualized on Clinisclect blue x-ray film (Carestream) or using ChemiDoc (Bio-Rad Laboratories).

Subcellular fractionation

Subcellular fractionation was performed on HeLa cells using the Peroxisome Isolation kit (PEROX1; Sigma-Aldrich). In brief, two 15-cm dishes of HeLa cells were transfected with either USP30-Flag, PMP34-USP30-Flag, or TOM20-USP30-Flag. Media was changed 8 h after transfection. Cells were washed, trypsinized, and collected 24 h following transfection. Cells were then re-suspended in Peroxisome Extraction Buffer (Sigma-Aldrich). The manufacturers' protocol was followed with the following exceptions: to lyse cells, a 5-mm metal cell homogenizer mechanically lysed the cells, and final fractions were pelleted at 200,000 g (Sargent et al., 2016). For this manuscript, an additional modification was made to the fraction collection. Fraction collection proceeded to separate the entirety of the gradient volume into six equal fractions (1–6; 20–27.5% iodixanol gradient). Pellets collected from each fraction were dissolved in 30 μl of lysis buffer (100 mM Tris-HCl and 1% SDS) and subsequently boiled in SDS-containing sample buffer. Finally, samples were Western blotted as described above. All blots were probed for Flag, PEX14, VAPB, and ATP5A.

Lysosome-targeting RG assay

The RG assay was performed as previously described (Deosaran et al., 2013). In brief, HeLa cells grown in Lab-Tek chambers were transfected with PEX26TM-RG and USP30-Flag 24–36 h before being subjected to amino acid starvation. Cells were either maintained in DMEM + FBS media or in HBSS without FBS. Both media were supplemented with 2 μM E-64 and 0.5 mM leupeptin. Cells were imaged live in CO₂-independent media

(Thermo Fisher Scientific) after 12-h incubation. Due to the necessity for live imaging, cells were unable to be costained for USP30-Flag expression. Efficiency of cotransfection of PEX26_{TM}-RG and USP30-Flag vectors was measured to be $94.6 \pm 2.9\%$.

Quantification and statistical analysis

Peroxisome density was quantified using Volocity software (version 6.3; Perkin Elmer). The total peroxisome number per cell was determined by drawing a region of interest (ROI) around individual cells and identifying PMP70 (red) punctate structures that meet a size and intensity cut-off controlled for background intensity. The same ROI was also used to determine the cell volume. Total peroxisome number within a cell was divided by the individual cell volume, producing the peroxisome density per cell. The average peroxisome density was calculated by averaging the peroxisome density from at least 30 cells. The relative peroxisome density was determined by normalizing the average peroxisome density per condition to that of the mock or nontargeting siRNA (siCTRL)-treated control sample. All Manders' colocalization coefficients (MCC) were calculated using Volocity for the portion of peroxisomes that colocalized with either USP30-Flag, PMP34-USP30-Flag, TOM20-USP30-Flag, or NBR1. As control for nonspecific colocalization between mitochondria and peroxisomes, mock-transfected cells were stained for endogenous PMP70 and the mitochondrial marker ATP5A. For all images, the same threshold was used for their MCC quantification. For all MCCs a minimum of 30 cells were counted per trial, with three trials quantified to determine statistical significance. Statistical significance was calculated using the Student's *t* test. Data distribution was assumed to be normal, but this was not formally tested.

For the quantification of the RG assay, the area of the cell was determined by drawing a ROI around an individual cell. Peroxisomes were identified by the PEX26_{TM}-RG construct expression, in which the total pixel intensity of GFP and RFP signal for each peroxisome and the area of each peroxisome were measured. The peroxisome with a total RFP signal that is three times higher than its GFP signal is considered as a "red peroxisome" and hence identified to be localized to the lysosome. The total area of "red" peroxisomes and the total area of peroxisomes were calculated and tabulated. Three independent trials were performed, and 50 cells were quantified in each treatment. The percentage of peroxisomes that colocalized with the lysosome in each cell was calculated and plotted.

Online supplemental materials

Fig. S1 shows the localization of USP30-Flag, PMP34-USP30-Flag, and TOM20-USP30-Flag in HeLa cells by immunofluorescence microscopy and subcellular fractionation. It also shows the localization of USP35-HA, TOM20-Cer, and FIS1-Myc in COS7 cells, costained for either endogenous PMP70 or overexpressing the mitochondrial marker OMP25-GFP. Fig. S2 shows the starvation-induced decrease in PEX14 protein upon overexpression of TOM20-USP30. It also shows the expression of all USP30 construct and siRNA validations by RT qPCR or Western blotting. Fig. S3 shows overexpression of PMP34-USP30 in HeLa

cells depleted of PEX1, the overexpression of USP30-Flag in PEX26-depleted HeLa cells, and the overexpression of PMP34-USP30 and USP30-Flag C77S in WT and PEX1 G843D fibroblasts.

Acknowledgments

We thank Sharon Leung for critically reading the manuscript.

This work was supported by the Canada Institute of Health Research grants (PJT156196 to P.K. Kim and MOP-130281 to G.A. McQuibban) and Natural Sciences and Engineering Research Council of Canada Discovery grants (RGPIN-2015-04077 to P.K. Kim and RGPIN-2015-05969 to G.A. McQuibban).

The authors declare no competing financial interests.

Author Contributions: P.K. Kim, G.A. McQuibban, Y. Wang and V. Riccio conceived the study. V. Riccio, N. Demers, R. Hua, M. Vissa, D.T. Cheng, and A.W. Strilchuk performed experiments. V. Riccio, N. Demers, R. Hua, and M. Vissa and P.K. Kim performed data analysis. V. Riccio and P.K. Kim wrote the manuscript. All authors contributed to the editing of the manuscript.

Submitted: 1 May 2018

Revised: 8 September 2018

Accepted: 11 January 2019

References

- Bingol, B., J.S. Tea, L. Phu, M. Reichelt, C.E. Bakalarski, Q. Song, O. Foreman, D.S. Kirkpatrick, and M. Sheng. 2014. The mitochondrial deubiquitinase USP30 opposes parkin-mediated mitophagy. *Nature*. 510:370-375. <https://doi.org/10.1038/nature13418>
- Braverman, N.E., G.V. Raymond, W.B. Rizzo, A.B. Moser, M.E. Wilkinson, E. M. Stone, S.J. Steinberg, M.F. Wangler, E.T. Rush, J.G. Hacia, and M. Bose. 2016. Peroxisome biogenesis disorders in the Zellweger spectrum: An overview of current diagnosis, clinical manifestations, and treatment guidelines. *Mol. Genet. Metab.* 117:313-321. <https://doi.org/10.1016/j.ymgme.2015.12.009>
- Cunningham, C.N., J.M. Baughman, L. Phu, J.S. Tea, C. Yu, M. Coons, D.S. Kirkpatrick, B. Bingol, and J.E. Corn. 2015. USP30 and parkin homeostatically regulate atypical ubiquitin chains on mitochondria. *Nat. Cell Biol.* 17:160-169. <https://doi.org/10.1038/ncb3097>
- Deosaran, E., K.B. Larsen, R. Hua, G. Sargent, Y. Wang, S. Kim, T. Lamark, M. Jauregui, K. Law, J. Lippincott-Schwartz, et al. 2013. NBR1 acts as an autophagy receptor for peroxisomes. *J. Cell Sci.* 126:939-952. <https://doi.org/10.1242/jcs.114819>
- Dixit, E., S. Boulant, Y. Zhang, A.S. Lee, C. Odendall, B. Shum, N. Hacohen, Z.J. Chen, S.P. Whelan, M. Fransen, et al. 2010. Peroxisomes are signaling platforms for antiviral innate immunity. *Cell*. 141:668-681. <https://doi.org/10.1016/j.cell.2010.04.018>
- Hua, R., S.K. Gidda, A. Aranovich, R.T. Mullen, and P.K. Kim. 2015. Multiple Domains in PEX16 Mediate Its Trafficking and Recruitment of Peroxisomal Proteins to the ER. *Traffic*. 16:832-852. <https://doi.org/10.1111/tra.12292>
- Klionsky, D.J., K. Abdelmohsen, A. Abe, M.J. Abedin, H. Abeliovich, A. Acevedo Arozena, H. Adachi, C.M. Adams, P.D. Adams, K. Adeli, et al. 2016. Guidelines for the use and interpretation of assays for monitoring autophagy (3rd edition). *Autophagy*. 12:1-222. <https://doi.org/10.1080/1548627.2015.1100356>
- Koch, A., Y. Yoon, N.A. Bonekamp, M.A. McNiven, and M. Schrader. 2005. A role for Fis1 in both mitochondrial and peroxisomal fission in mammalian cells. *Mol. Biol. Cell*. 16:5077-5086. <https://doi.org/10.1091/mbc.e05-02-0159>
- Kuma, A., M. Hatano, M. Matsui, A. Yamamoto, H. Nakaya, T. Yoshimori, Y. Ohsumi, T. Tokuhisa, and N. Mizushima. 2004. The role of autophagy during the early neonatal starvation period. *Nature*. 432:1032-1036. <https://doi.org/10.1038/nature03029>

- Law, K.B., D. Bronte-Tinkew, E. Di Pietro, A. Snowden, R.O. Jones, A. Moser, J. H. Brumell, N. Braverman, and P.K. Kim. 2017. The peroxisomal AAA ATPase complex prevents pexophagy and development of peroxisome biogenesis disorders. *Autophagy*. 13:868–884. <https://doi.org/10.1080/15548627.2017.1291470>
- Liang, J.R., A. Martinez, J.D. Lane, U. Mayor, M.J. Clague, and S. Urbé. 2015. USP30 deubiquitylates mitochondrial Parkin substrates and restricts apoptotic cell death. *EMBO Rep*. 16:618–627. <https://doi.org/10.15252/embr.201439820>
- Marcassa, E., A. Kallinos, J. Jardine, E.V. Rusilowicz-Jones, A. Martinez, S. Kuehl, M. Islinger, M.J. Clague, and S. Urbé. 2018. Dual role of USP30 in controlling basal pexophagy and mitophagy. *EMBO Rep*. 19:e45595. <https://doi.org/10.15252/embr.201745595>
- Nakamura, N., and S. Hirose. 2008. Regulation of mitochondrial morphology by USP30, a deubiquitinating enzyme present in the mitochondrial outer membrane. *Mol. Biol. Cell*. 19:1903–1911. <https://doi.org/10.1091/mbc.e07-11-1103>
- Nordgren, M., B. Wang, O. Apanasets, and M. Fransen. 2013. Peroxisome degradation in mammals: mechanisms of action, recent advances, and perspectives. *Front. Physiol*. 4:145. <https://doi.org/10.3389/fphys.2013.00145>
- Nordgren, M., T. Francisco, C. Lismont, L. Hennebel, C. Brees, B. Wang, P. P. Van Veldhoven, J.E. Azevedo, and M. Fransen. 2015. Export-deficient monoubiquitinated PEX5 triggers peroxisome removal in SV40 large T antigen-transformed mouse embryonic fibroblasts. *Autophagy*. 11:1326–1340. <https://doi.org/10.1080/15548627.2015.1061846>
- Nuttall, J.M., A.M. Motley, and E.H. Hettema. 2014. Deficiency of the exportomer components Pex1, Pex6, and Pex15 causes enhanced pexophagy in *Saccharomyces cerevisiae*. *Autophagy*. 10:835–845. <https://doi.org/10.4161/auto.28259>
- Rambold, A.S., B. Kostecky, N. Elia, and J. Lippincott-Schwartz. 2011. Tubular network formation protects mitochondria from autophagosomal degradation during nutrient starvation. *Proc. Natl. Acad. Sci. USA*. 108:10190–10195. <https://doi.org/10.1073/pnas.1107402108>
- Sargent, G., T. van Zutphen, T. Shatseva, L. Zhang, V. Di Giovanni, R. Bandsma, and P.K. Kim. 2016. PEX2 is the E3 ubiquitin ligase required for pexophagy during starvation. *J. Cell Biol*. 214:677–690. <https://doi.org/10.1083/jcb.201511034>
- Schrader, M., J.L. Costello, L.F. Godinho, A.S. Azadi, and M. Islinger. 2016. Proliferation and fission of peroxisomes - An update. *Biochim. Biophys. Acta*. 1863:971–983. <https://doi.org/10.1016/j.bbamcr.2015.09.024>
- Smith, J.J., and J.D. Aitchison. 2013. Peroxisomes take shape. *Nat. Rev. Mol. Cell Biol*. 14:803–817. <https://doi.org/10.1038/nrm3700>
- Trompier, D., A. Vejux, A. Zarrouk, C. Gondcaille, F. Geillon, T. Nury, S. Savary, and G. Lizard. 2014. Brain peroxisomes. *Biochimie*. 98:102–110. <https://doi.org/10.1016/j.biochi.2013.09.009>
- Wanders, R.J., and H.R. Waterham. 2006. Biochemistry of mammalian peroxisomes revisited. *Annu. Rev. Biochem*. 75:295–332. <https://doi.org/10.1146/annurev.biochem.74.082803.133329>
- Wang, W., and S. Subramani. 2017. Role of PEX5 ubiquitination in maintaining peroxisome dynamics and homeostasis. *Cell Cycle*. 16:2037–2045. <https://doi.org/10.1080/15384101.2017.1376149>
- Wang, Y., M. Serricchio, M. Jauregui, R. Shanbhag, T. Stoltz, C.T. Di Paolo, P. K. Kim, and G.A. McQuibban. 2015. Deubiquitinating enzymes regulate PARK2-mediated mitophagy. *Autophagy*. 11:595–606. <https://doi.org/10.1080/15548627.2015.1034408>
- Yamashita, S., K. Abe, Y. Tatemichi, and Y. Fujiki. 2014. The membrane peroxin PEX3 induces peroxisome-ubiquitination-linked pexophagy. *Autophagy*. 10:1549–1564. <https://doi.org/10.4161/auto.29329>
- Youle, R.J., and D.P. Narendra. 2011. Mechanisms of mitophagy. *Nat. Rev. Mol. Cell Biol*. 12:9–14. <https://doi.org/10.1038/nrm3028>
- Zhang, J., D.N. Tripathi, J. Jing, A. Alexander, J. Kim, R.T. Powell, R. Dere, J. Tait-Mulder, J.H. Lee, T.T. Paull, et al. 2015. ATM functions at the peroxisome to induce pexophagy in response to ROS. *Nat. Cell Biol*. 17:1259–1269. <https://doi.org/10.1038/ncb3230>